J. of Thermal Science Vol.9, No.1

Effect of Nonequilibrium Condensation of Moist Air on Transonic Flow Fields

Katsumi Shimamoto Shigeru Matsuo Toshiaki Setoguchi

Department of Mechanical Engineering, Saga University, 1, Honjo-machi, Saga-shi, Saga, 840-8502, Japan

When condensation occurs in a supersonic flow field, the flow is affected by the latent heat released. In the present study, a condensing flow was produced by an expansion of moist air in nozzle with circular bump models and shock waves occurred in the supersonic parts of the flow fields. The experimental investigations were carried out to show the effects of initial conditions in the reservoir and nozzle geometries on the shock wave characteristics and the turbulences in the flow fields. Furthermore, in order to clarify the effect of condensation on the flow fields with shock waves, Navier-Stokes equations were solved numerically using a 3rd-order MUSCL type TVD finite-difference scheme with a second order fractional step for time integration. As a result, the effect of condensation on the aspect of flow field has been clarified.

Keywords: compressible flow, condensation, boundary layer, control of shock wave, moist air, wavelet transform

Introduction

Many studies on condensation occurring in the case of the rapid expansion of moist air or steam in a supersonic nozzle have been performed experimentally and numerically, and the characteristics of condensation have been nearly clarified[1-4]. Schnerr et al.[5] and Iriya et al.[6] investigated the effect of condensation on the strength of shock wave on surface of wing, drag and lift numerically. However, the effect of condensation on the shock wave on surface of wing and turbulences behind shock wave has not yet been clarified satisfactorily.

Phenomena which become the subject of the present study are essentially the same as the passive control[7] of shock-boundary layer using the porous wall with a cavity underneath. Therefore, it is expected that the reduction of Mach number due to nonequilibrium condensation just before shock wave suppresses the separation of boundary layer generated by shock wave, and droplets generated by condensation suppress the fluctuation of flow field due to the shock wave. In the meanwhile, total pressure of the flow is reduced by condensation[8] and it seems that this reduction affects the interaction of shock wave with boundary layer. However, study for phenomena like these has not yet been conducted in detail.

In the present study, a condensing flow was produced by an expansion of moist air in the nozzle with circular bump models and shock waves occurred in the supersonic parts of the flow fields. The experimental investigations were carried out to show the effects of initial conditions in the reservoir and nozzle geometries on the characteristics of the shock wave and the turbulences in the flow fields. Furthermore, in order to clarify the effect of condensation on the flow fields with shock waves, Navier-Stokes equations were solved numerically using a 3rd-order MUSCL type TVD finite-difference scheme with a second order fractional step for time integration.

Received 2000

Nomenclature

Mn	Mach number [-]	$\bar{r}$	average radius of droplet [m]
M	molecular weight [kg/kmol]	s	entropy [J/K]
R	radius [m]	t	time [s]
S	supersaturation (p_v/p)		**Greeks**
T	temperature [K]	γ	ratio of specific heats [-]
$W(b,a)$	wavelet coefficient	σ	surface tension [N/m]
a	scale parameter	ω	specific humidity
b	shift parameter	ρ	density [kg/m^3]
c_p	specific heat at constant pressure of mixture [J/(kg·K)]	ψ	mother wavelet
g	condensate mass fraction [-] ($=m_l/(m_a+m_v+m_l)$		**Subscripts**
l	length of bump model [m]	0	stagnation state
m	mass [kg]	01	stagnation state at nozzle entrance
p	pressure [Pa]	a	air
$p(t)$	pressure time history [Pa]	l	liquid
p_s	saturated vapour pressure [Pa]	m	mixture
$\Re$	universal gas constants [J/(kg·K)]	max	maximum
		v	vapour

Experimental Apparatus and Procedure

A supersonic indraft wind tunnel[9] where dry air at atmospheric pressure was drawn into a vacuum tank, was used in the present experiment. Fig.1 shows the details of test section. Half nozzles of radius R=40, 200 mm with a thickness 4 mm were set at the lower wall in the test section. The chord length l of bump model for R=40 mm and 200 mm are 34.9 mm and 76.9 mm, respectively. The pressure measurements were conducted by a pressure transducer (TOYODA, PMS-5H) mounted on the pressure holes (ϕ1 mm) on the bump model. Power spectrum density distributions, amplitudes of oscillation And wavelet transform[10] were obtained by using

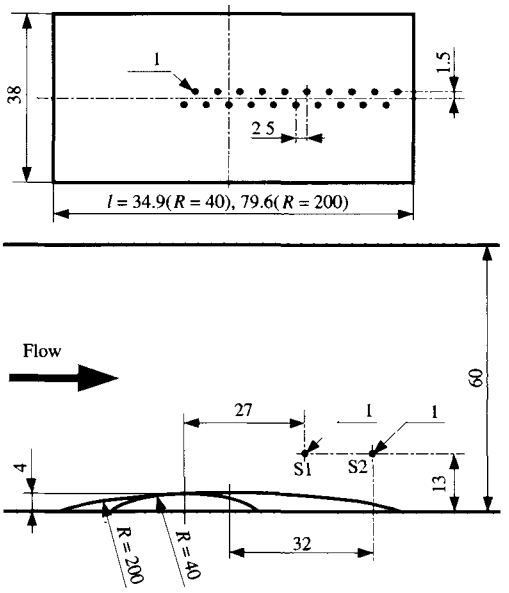

Fig.1 Details of test section

pressure data at positions (S1, S2) behind a shock wave. The flow field was also investigated by a schlieren optical method, and shear sensitive liquid crystal (MERCK Industrial Chemicals, TI622) was used for flow visualization on surface of bump model.

The experimental procedure is as follows. At first, dry air is charged into reservoir through silica gel box at atmospheric pressure. Then, the stagnation temperature and the relative humidity in reservoir were measured with a thermometer and a humidity indicator (Vaisala, HM-34), respectively. The supersonic steady flow lasting about 5 seconds was obtained in the test section.

The stagnation pressure p_{01} of moist air in the reservoir is 102 kPa, and the stagnation temperature T_{01} is set at 298 K. The initial degree of supersaturation S_{01}, which is the ratio of vapor pressure to the equilibrium saturation pressure corresponding to the inlet temperature, can be changed from 0.24 to 0.80. The pressure upstream of bump model p/p_{01} is 0.719 (Mn=0.735).

Numerical Procedures

Governing Equations

Assumptions using in the present calculation[11] of two phase flows are as follows:

1. No velocity slip exists between condensate particles and gas mixture.

2. No temperature difference exists between condensate particles and gas mixture.

3. Effect of the condensate particles on pressure is neglected.

The governing equations under consideration are the unsteady two-dimensional compressible Navier-Stokes

equations and droplet growth equation[12] written in the Cartesian coordinate system (x,y). In order to obtain the normalized conservation equations, all variables are non-dimensionalized with reference values.

Values of accommodation coefficient for nucleation[13], condensation coefficient[14] and coefficient of surface tension[15] used in the present calculations, are 10^6, 0.9 and 1.29, respectively. Baldwin-Lomax model[16] was used as a turbulence model in the computations.

In the present study, governing systems are mapped from the physical plane of reference (x,y) into a computational plane of reference (ξ,η) with general transformations. Furthermore, in order to solve the set of above equations, 3rd-order MUSCL type TVD finite-difference scheme[17] with a second-order fractional-step for time integration are adopted to the flow equations and the droplet growth equation and a second-order centered difference scheme is used for viscous terms.

Initial and Boundary Conditions

The initial degree of supersaturation S_{01} and total temperature T_{01} in the reservoir are used for initial conditions. Total pressure in the reservoir is set at p_{01}=102kPa. Pressure at the upstream of the model is set at p/p_{01}=0.719 (M_n=0.735).

The supersonic nozzle geometry of computational grid is shown in Fig.2. The nozzle has a height of 60 mm at the inlet and exit, a radius of circular arc R (characteristics length)=40 mm and a height of nozzle throat 56 mm. The grids contain 100 divisions in ξ direction and 50 divisions in η direction. The highest and lowest lines are solid boundaries and the minimum dimensional length is 7.17×10^{-2} mm at the near wall of solid boundaries.

Inlet and exit boundaries are constrained with free boundary condition. Non-slip velocity, iso-pressure $(\partial p/\partial \eta = 0)$ and no heat transfer $(\partial T/\partial \eta = 0)$ are constrained on the solid wall. Condensate mass fraction $g(=m_l/(m_a+m_v+m_l))$ is set at g=0 on the wall. Vector of the conservative variables at a fictitious cell at inlet and exit is constrained with Riemann invariant. The value of CFL number is 0.98.

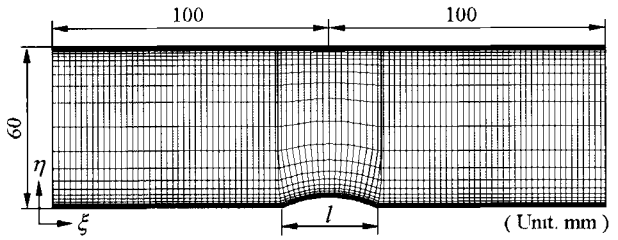

Fig.2 Calculation Grid

Results and Discussion

Flow Visualization and Pressure measurement

Figs.3(a) and (b) show schlieren photographs in cases of R=40 mm and 200 mm for S_{01}=0.240.80, respectively. Flow direction is left to right. As seen from these figures, a shock wave is clearly visible for S_{01}=0.24 (dry air). With increase of S_{01}, it seems that the strength of shock wave becomes weak and the position of shock wave moves upstream. This is due to reduction of Mach number just before the shock wave by condensation.

Figs.4(a) and (b) show photographs of oil flow pattern on the bump wall obtained by shear sensitive liquid crystal in cases of R=40 mm and 200 mm, respectively. In Fig.4(a), separation of boundary layer

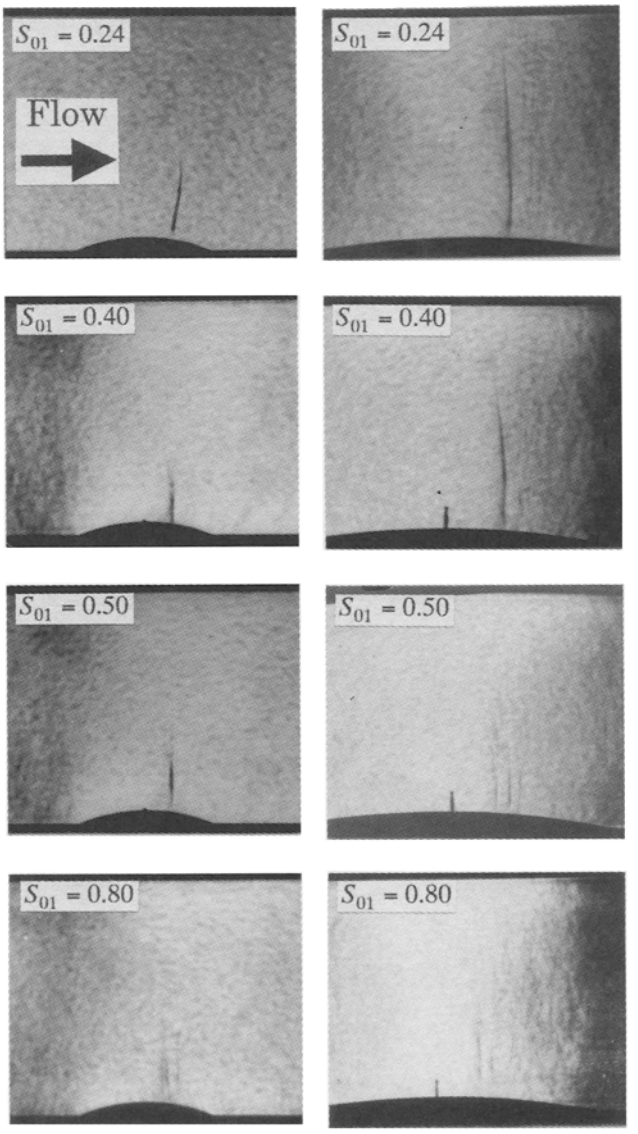

(a) R = 40 mm (b) R = 200 mm

Fig.3 Schlieren photographs

occurs behind the shock wave and the flow field is complicated for S_{01}=0.24. However, it can be seen that the separation of boundary layer is suppressed with the increase of S_{01}. In Fig.3(b), a shock wave exists in the flow field for S_{01}=0.24. But, in Fig.4(b), separation of boundary layer does not occur behind the shock wave and the flow field does not change significantly.

Figs.5(a) and (b) show pressure distributions on the bump wall in cases of R=40 mm and 200 mm for S_{01}=0.24~0.80, respectively. The abscissa is the distance x measured from the nozzle throat divided by the chord length of bump model l, and for the ordinate, the local static pressure p is represented in non-dimensional form divided by the initial total pressure p_{01}. As seen from these figures, gradients of pressure distributions in the position close to shock wave (R=40 mm : x/l=0.172, R=200 mm : x/l=0.214) are large in case of S_{01}=0.24, and with increase of S_{01}, the position of shock wave moves upstream and the gradients become smaller. This shows that nonequilibrium condensation occurred upstream of shock wave is likely to suppress separation of boundary layer due to shock wave. Furthermore, in Fig.5(a), it can be seen that recovery of pressure is improved due to suppression of the separation with increase of S_{01}.

In the previous study, it is evident that total pressure of the flow decreases by condensation with increase of S_{01}[1,8]. However, in case with separation of boundary layer (Fig.3(a) and Fig.4(a)), it is considered that with the increase of S_{01}, the effect of a reduction of loss due to pressure recovery behind the shock wave becomes strong in comparison with the increase of total pressure loss by condensation in the region close to the throat (x/l = 0~0.2), and total pressure loss of the flow field becomes small.

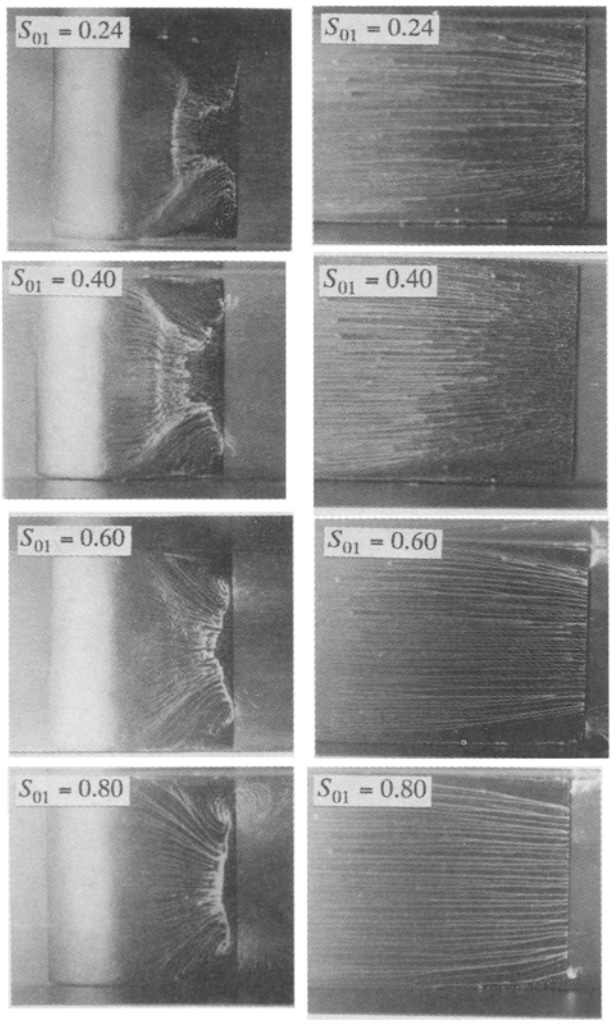

(a) R = 40 mm (b) R = 200 mm

Fig.4 Flow patterns on nozzle surface using liquid crystal

Effect of Condensation on Pressure Fluctuation on the Wall

Figs.6(a) and (b) show root mean square values p_{rms} of pressure variations corresponding to Figs.5(a) and (b),

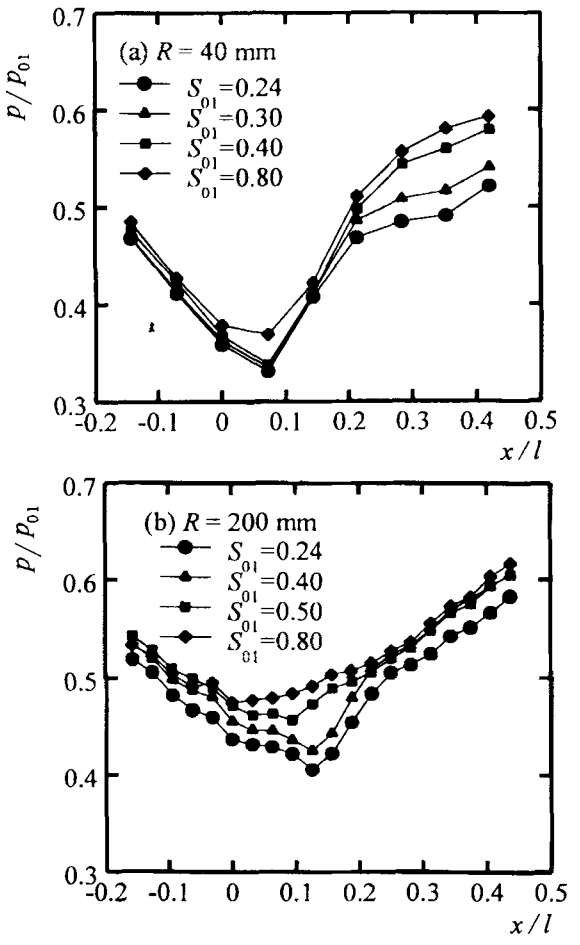

Fig.5 Pressure distributions

respectively. On the ordinate, p_{rms} on the bump wall is represented in non-dimensional form divided by the mean values p_{av} of pressure variations. As seen from these figures, values of p_{rms} are the largest at the position (R=40 mm : x/l=0.172, R=200 mm : x/l=0.214) of shock wave in case of S_{01}=0.24, and with the increase of S_{01}, peaks of p_{rms} become smaller. Furthermore, the position of shock wave and the peak of p_{rms} move upstream with increase of S_{01}.

From the result as described above, it is concluded that pressure variations on the bump wall in the region that shock wave exists are suppressed by condensation. The reasons are considered that it is due to the effect of small droplets generated by condensation and degree of interaction of shock wave with boundary layer becomes weak due to reduction of the strength of shock wave with increase of S_{01}[11].

Effect of Condensation on Pressure Fluctuation behind Shock Wave

Informations on time and frequency of a signal can be 4obtained using the continuous wavelet transform. This transform that has the advantage on the analysis of unsteady data, can obtain local informations in the region of time. In the present study, continuous wavelet transform was applied to pressure variations behind the shock wave.

The continuous wavelet transform $W(b,a)$ for a pressure signal $p(t)$ with time t is defined as follows :

$$W(b,a)=\frac{1}{a^{1/2}}\int_{-\infty}^{\infty}\psi\left(\frac{t-b}{a}\right)p(t)dt \qquad (1)$$

where ψ is a mother wavelet, and a is the scale and b implies location on the t axis. The wavelet transform (coefficient) $W(b, a)$ plotted in the (b, a) space describes the multi-scale structure of the pressure signal $p(t)$. The mother wavelet that is Morley wavelet[10], is defined as follows :

$$W(t)=(b,a)=\exp(ik_{\psi}T)\exp\left(-\frac{T^2}{2}\right) \qquad (2)$$

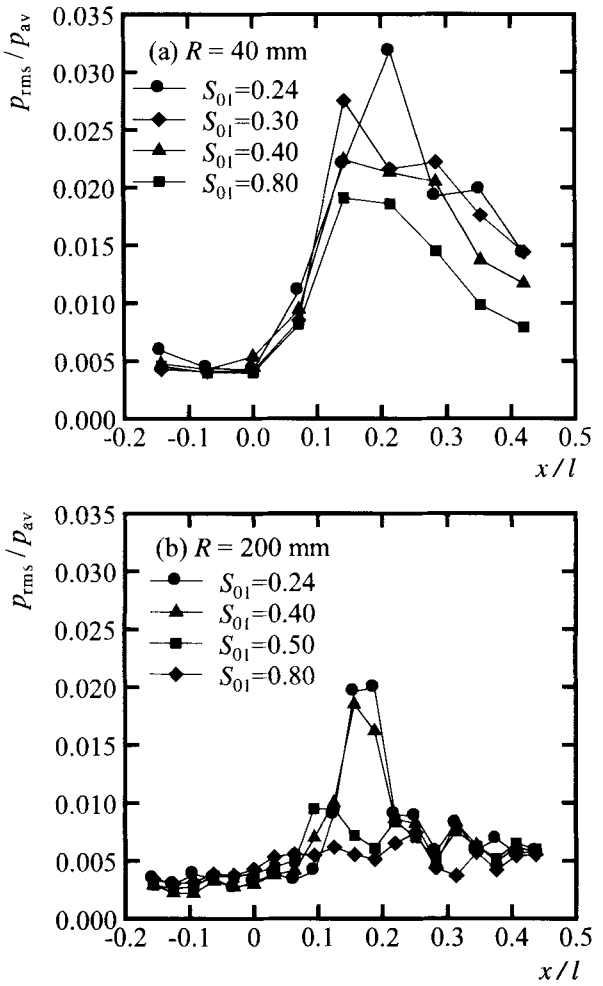

Fig.6 RMS values of pressure variations

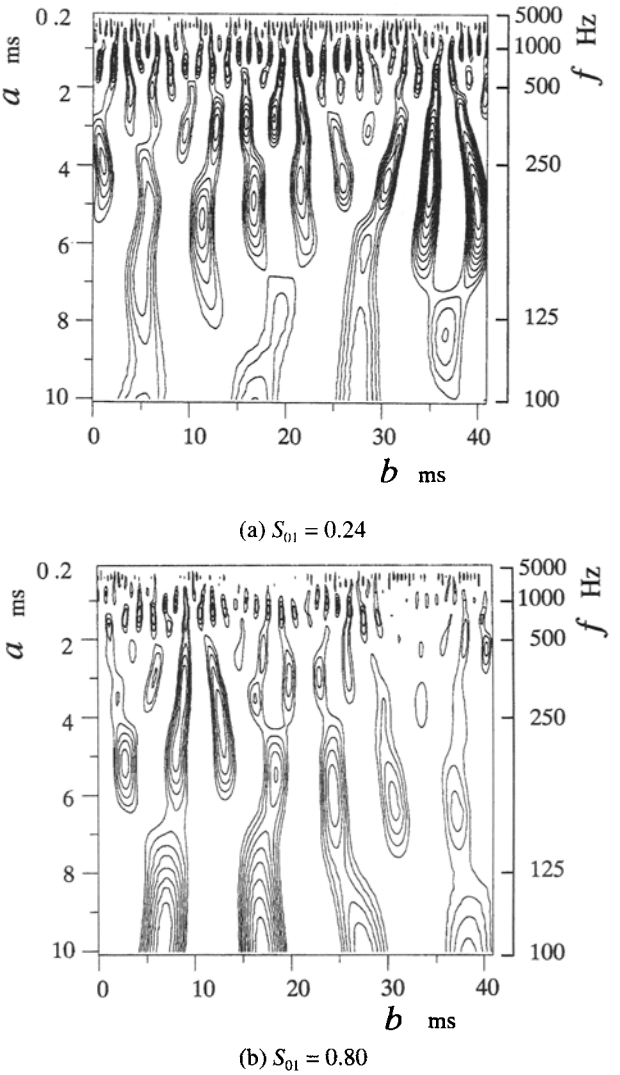

Fig.7 Continuous wavelet transforms (R =40 mm)

$$T = \frac{t-b}{a} \tag{3}$$

where k_ψ is a numerical constant (k_ψ=6), and i implies $\sqrt{-1}$. The real part of the Morley wavelet is symmetric with respect to T=0. The value of $1/a$ is taken to be the same as frequency.

Figs.7 and 8 show the relationship between S_{01} and the wavelet coefficient $W(a,b)$ obtained from the pressure signal $p(t)$ in the (a,b) parameter space in cases of R=40 mm and 200 mm, respectively. Measuring points for R=40 mm and 200 mm are S1 and S2 as shown in Fig.1, respectively. The abscissa is the time b (shift parameter). The left and right ordinates are the scale parameter a and frequency f, respectively. Contour lines are indicated for W = 0 and their intervals are equal in each figures.

Figs.7 and 8 show that dense regions of contour lines exist at equal intervals on the b-axis in the range from high to low frequency in case of S_{01}=0.24. The existence of dense region for high frequency is due to separation of boundary layer. In case of S_{01}=0.80, contour lines in the region of high frequency become sparse except in the region of low frequency. This fact means that occurrence of condensation suppresses especially high frequency oscillation.

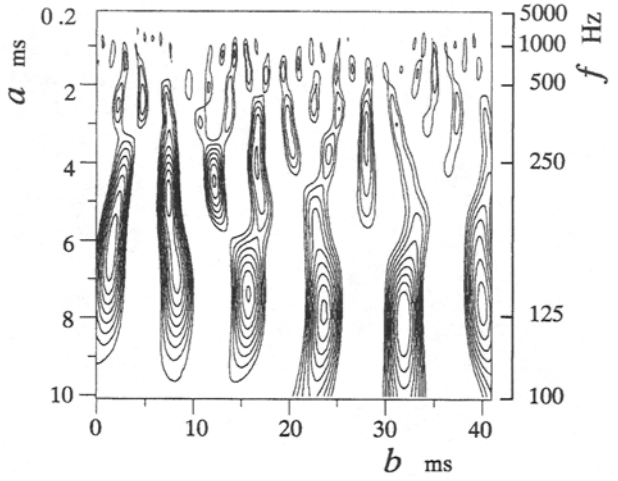

(a) S_{01} = 0.24

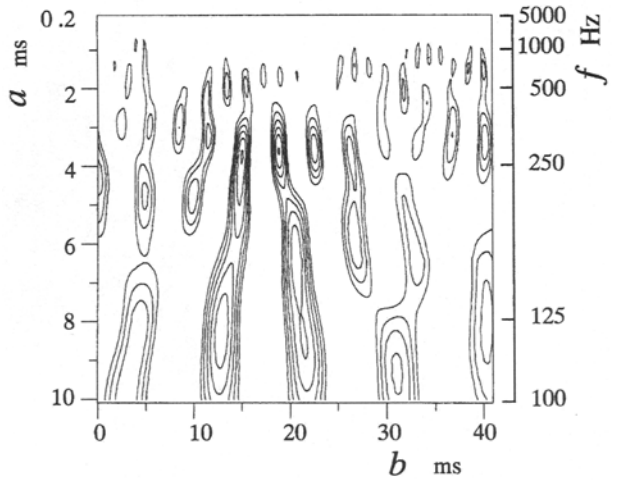

(b) S_{01} = 0.80

Fig.8 Continuous wavelet transforms (R =200 mm)

Simulation Results and Total Pressure Loss

Fig.9 shows pressure distributions on the curved wall obtained by calculations in the case of R=40 mm, together with the experimental results. The simulated results are compared with experimental data in reasonable agreement, and the position of shock wave moves upstream with the increase of S_{01}.

In cases of S_{01}=0.24, 0.40, 0.60 for R=40 mm, contour maps of Mach number M_n are shown in Figs.10(a)~(c). As is evident from these figures, the strength of shock wave becomes weak with increase of S_{01} and separation of boundary layer is suppressed slightly. From these results and pressure distributions shown in Fig.5, the present simulation using a turbulence model is effective for the transonic flow field with condensation.

Figs.11(a)~(c) show contour maps of coefficient ($1 - p_0/p_{01}$) of total pressure loss. The following equation[18] was used in order to obtain total pressure loss.

$$\begin{aligned} s - s_{01} = {} & (1-\omega_{01})\frac{\Re}{Ma}\ln\left(T^{(\gamma_a/(\gamma_a-1))}\right) \\ & + (\omega_{01}-g)\frac{\Re}{M_v}\ln\left(T^{(\gamma_v/(\gamma_v-1))}/p_v\right) \\ & + g\left(-\frac{1}{\bar{r}}\frac{3}{\rho_l}\frac{\partial\sigma}{\partial T}\right) \end{aligned} \tag{4}$$

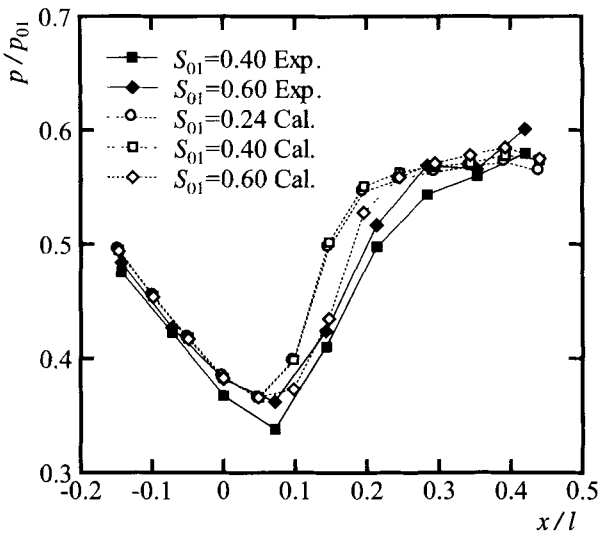

Fig.9 Pressure distributions (R = 40 mm)

$$\frac{s-s_{01}}{c_p}=\ln\left(\frac{T_0}{T_{01}}\right)-\frac{\Re}{M_m c_p}\ln\left(\frac{p_0}{p_{01}}\right) \tag{5}$$

The region that total pressure loss occurs, expands with increase of S_{01}. As a result, increase of S_{01} brings reduction of the strength of shock wave and suppression of separation of boundary layer. However, in case that energy loss in the whole flow field is estimated, the special attention should be paid to total pressure loss occurred by condensation.

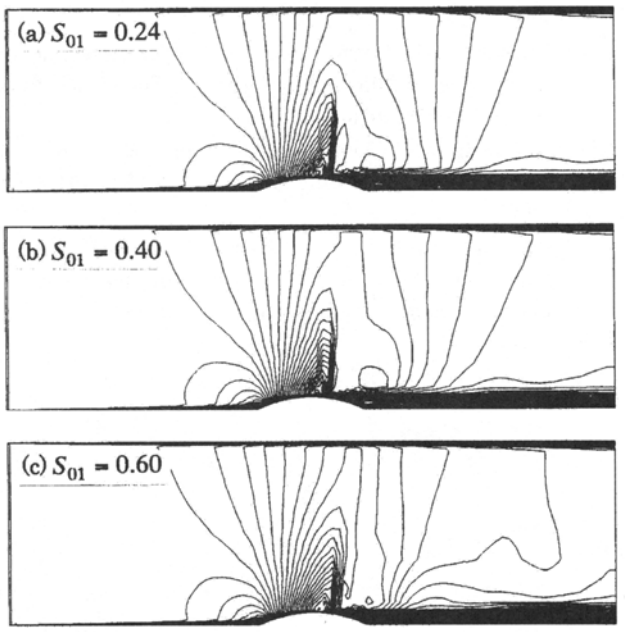

Fig.10 Contour maps of Mach number (R = 40 mm)

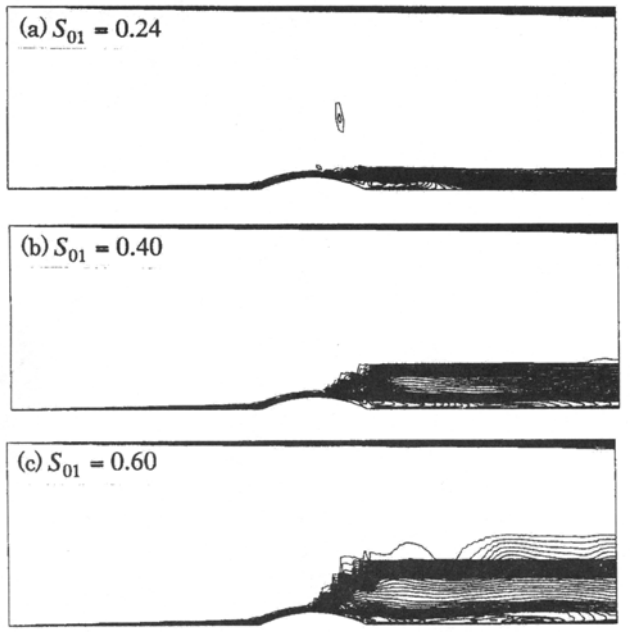

Fig.11 Contour maps of total pressure loss (R = 40 mm)

Conclusions

In the condensing flow produced by an expansion of moist air in nozzle with circular bump models, shock waves occurred in the supersonic parts of the flow fields. Experimental and numerical investigations were carried out to clarify the effects of initial conditions in the reservoir and nozzle geometries on the characteristics of shock wave and the turbulences in the flow fields. The results obtained are summarized as follows:

1. In case that boundary layer separates for initial degree of supersaturation S_{01}=0.24, the separation is suppressed with increase of S_{01}.

2. Gradients of pressure distributions are large in case of S_{01}=0.24, and with increase of S_{01}, the position of shock wave moves upstream and the gradients become small.

3. With increase of S_{01}, the strength of shock wave becomes weak and the values of p_{rms} in the region that shock wave exists become small. Furthermore, fluctuations from low to high frequency are contained in pressure variations behind the shock wave and the fluctuation of high frequency is especially suppressed with increase of S_{01}.

4. The simulated results using a turbulence model are compared with experimental data in reasonable agreement and suppression of separation of boundary layer has been confirmed with the increase of S_{01}. Furthermore, the region that total pressure loss occurs, expands with increase of S_{01}.

References

[1] Wegener, P.P., Mach, L.M.. "Condensation in Supersonic Hypersonic Wind Tunnels," Adv. in Appl Mech., **.5**, pp.307-447, Academic Press., (1958).

[2] Matsuo, K., Kawagoe, S., Sonoda, K. and Sakao, K.. "Studies of Condensation Shock Waves (Part 1, Mechanism of their Formation)," Bulletin of JSME, **28**, No.241, pp.1416-1422, (1985).

[3] Zierep , J., Lin , S.. "Bestimmung des Kondensationsbeginns Kondensation Bei Entspannung feuchter Luft in Ueberschallduesen," Forsch. Ing. Wes., **.33**, pp.169-172, (1967).

[4] Schnerr, G.H.. "Homogene Kondensation in Stationaeren Transsonischen Stroemungen durch Laval-duesen und um Profile," Hab. schrift, Universitaet Karlsruhe, (1986).

[5] Schnerr, G.H., Dohrmann, U.. "Transonic Flow Around Airfoils with Relaxation and Energy Supply by Homogeneous Condensation," AIAA Journal., **28**, No.7, pp.1187-1193, (1990).

[6] Iriya, A., Yamamoto, S. and Daiguji, H.. "Numerical Method for Transonic Viscous Flow Considering Humidity," Transaction of JSME, **62**, No.603, pp.3854-3859, (1996).

[7] Bahi, L., Ross, J.M. and Nagamatsu, H.T.. "Passive Shock Wave/Boundary Layer Control for Transonic Airfoil Drag Reduction," AIAA-83-0137, (1983).

[8] Kwon, S.B., Matsuo, K., Kawagoe, S. and Matsuo, S.. "Total Pressure Loss in Supersonic Nozzle Flows with Condensation (Numerical Analyses)," JSME International Journal, Ser.2, **31**, No.1, pp.16-21, (1988).

[9] Matsuo, S., Zeutzius, M., Setoguchi, T. and Kaneko, K.. "Investigation of Supersonic Cavity Flow with Pressure Oscillation," Proc. of Int. Conf. on Fluid Eng., **3**, pp.1473-1478, (1997).

[10] Farge, M.. "Wavelet Transforms, Their Applications to Turbulence," Annu. Rev. Fluid Mech., **24**, pp.395-457, (1992).

[11] Matsuo, S., Setoguchi, T., Yu, S. and Hirahara, H.. "Effect of Nonequilibrium Condensation of Moist Air on the Boundary Layer in a Supersonic Nozzle," Journal of Thermal Science, **6**, No.4, pp.260-272, (1997).

[12] Sislian, J.P.. "Condensation of Water Vapour with or without a Carrier Gas in a Shock Tube," UTIAS Rep.201, (1975).

[13] Wegener, P.P.. Wu, B., Nucleation Phenomena, pp.325, (1977).

[14] Mills, A.F., Seban, R.A.. "The Condensation Coefficient of Water," Int. J. Heat Mass Transfer, **10**, pp.1815-1827, (1967).

[15] Kirkwood, J.G., Buff, F.P.. "The Statistical Mechanical Theory of Surface Tension," J. Chem. Phys., **17**, pp.3389-3343, (1949).

[16] Baldwin, B.S., Lomax, H.. "Thin Layer Approximation and Algebraic Model for Separated Turbulent Flows," AIAA-78-257, (1978).

[17] Yee, H.C., "A Class of High-Resolution Explicit and Implicit Shock-Capturing Methods," NASA TM-89464, (1989).

[18] Sugawara, M., Oshima, N.. "Analysis of Condensation in Supersonic Nozzles," Proc. of 12th Int. Sym. on Combustion, pp.1193-1201, (1968).